Chemical Engineering Journal Advances 26 (2026) 101150

Contents lists available at ScienceDirect

Chemical Engineering Journal Advances

journal homepage: www.sciencedirect.com/journal/chemical-engineering-journal-advances

Iso-butanol production as a sustainable chemical from renewable methanol/ethanol upgrading using Ni/Cu-Al hydrotalcite-derived catalysts under mild conditions

Quoc Khanh Tran [a,*], Justus Hüging [a], Joachim Pasel [a], Ralf Peters [a,b]

[a] Institute of Energy Technologies, IET-4: Electrochemical Process Engineering, Forschungszentrum Jülich GmbH, Jülich 52425, Germany
[b] Synthetic Fuels, Faculty of Mechanical Engineering, Ruhr-Universität Bochum, Universitätsstr. 150, Bochum 44801, Germany

ARTICLE INFO

Keywords:
Iso-butanol (i-BuOH)
Higher alcohols
Hydrotalcite
Ni catalyst

ABSTRACT

Iso-butanol (i-BuOH) is a high-value bio-derived alcohol with significant potential as a renewable fuel and chemical intermediate. Sustainable production of i-BuOH is made possible by the Guerbet reaction, which presents a viable pathway for the selective conversion of ethanol into higher alcohols. In this work, we examine the catalytic performance of various Ni/Cu-Al hydrotalcite-derived catalysts for the synthesis of i-BuOH from a methanol/ethanol mixture. Via Guerbet reaction, the mixture of methanol/ethanol mainly converts into i-BuOH and small amounts of 1-propanol, 2-methyl-butanol, and 2-methyl-pentanol. The experiment with a 5.0 wt% loading of Ni_{10}/2Cu-Al catalyst at 185 °C, 6 bar N_2 and 4 h reaction time exhibits exceptional activity, producing 100% selectivity toward higher alcohols (C_3—C_6) with 156.4 mmol/L i-BuOH (85.8% selectivity), 11.4% ethanol conversion, and space-time yield of 7.6 $mmol.g^{-1}.h^{-1}$, respectively. The catalyst's active sites of Ni and Cu species, which encourage the dehydrogenation/re-hydrogenation, and formation of C–C bonds and improve the efficiency of the methanol/ethanol coupling process, are responsible for its exceptional performance. Moreover, the Cu-Al hydrotalcite-derived structure offers stable and adjustable support, promoting selective product generation and reducing side reactions. The knowledge gathered from this research helps to create effective catalytic systems that convert bio-alcohols into renewable fuels and value-added chemicals as well as understanding the reaction pathways of methanol/ethanol coupling. This opens the door to more carbon neutrality for producing chemicals and energy.

1. Introduction

Iso-butanol (i-BuOH) is an important bio-based chemical with diverse applications in renewable energy, industrial solvents, and chemical synthesis (Scheme 1) [1,2]. As a renewable biofuel, it offers advantages over ethanol, including higher energy density, lower volatility, and reduced water absorption, making it a superior gasoline additive with better fuel stability and infrastructure compatibility [3]. In the chemical industry, i-BuOH serves as a key precursor for value-added compounds such as butene, butadiene, and isobutyl acetate, which are widely used in polymer production, coatings, and pharmaceuticals. Additionally, its role as an industrial solvent makes it valuable in paints, inks, adhesives, and fragrances due to its favorable solubility properties. Beyond these applications, i-BuOH also shows potential as a component of aviation and marine fuels, offering high energy content and reduced carbon emissions [4].

The sustainable production of i-BuOH from bio-alcohols, such as ethanol, and methanol via the Guerbet reaction, represents an environmentally friendly approach to reducing the dependence on fossil-derived chemicals while promoting the transition toward greener energy and chemical processes [5,6]. The Guerbet reaction presents a viable route for the conversion of ethanol to higher alcohols in the quest for sustainable energy and chemical production [6,7]. Long chain alcohols, especially i-BuOH, are useful in industry as a fuel additive, solvent, and starting point for many other compounds [8]. Higher alcohols and water are produced by the condensation and dehydrogenation of alcohols via Guerbet reaction. This reaction provides a mechanism to create longer-chain alcohols with desirable characteristics in addition to allowing the valorization of ethanol, a widely available renewable resource that is frequently generated from biomass. In the Guerbet

* Corresponding author.
E-mail address: Qu.tran@fz-juelich.de (Q.K. Tran).

https://doi.org/10.1016/j.ceja.2026.101150

Available online 21 March 2026

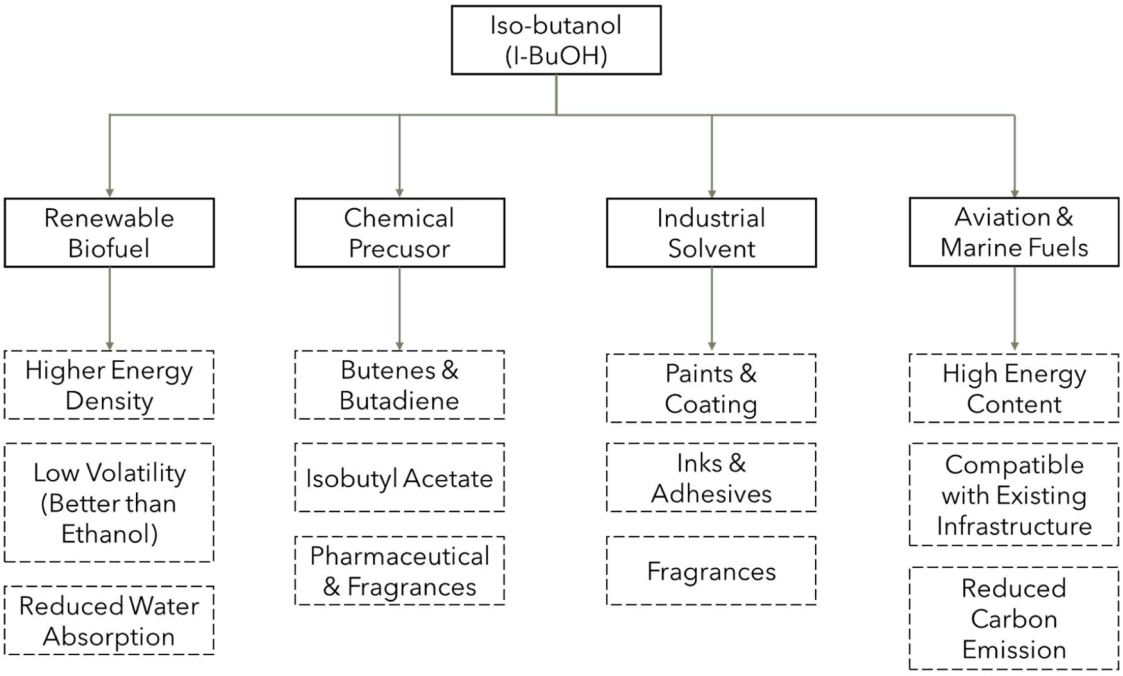

Scheme 1. The role of i-BuOH in various applications.

reaction, efficient catalysts are essential for the dimerization of lower alcohols, and many catalysts have demonstrated promise in this respect. Sama et al. [9] produced over 50% i-BuOH yield with >90% selectivity in 2 h reaction time using Ru-coordinated dppen (1,1-bis(diphenylphosphino)ethylene). Liu et al. [10] used various Mn-pincer (PNP) catalysts to convert methanol/ethanol mixture into i-BuOH at 160 °C and 16 h of reaction time with the conversion of 34–38%. King et al. [11] reached 97% selectivity and 35% yield of i-BuOH using Ru-pincer complexes at 180 °C and 18 h reaction time. While the use of homogeneous catalysts for i-BuOH production has proven effective, the separation process of liquid products as well as recycling remain challenge, requiring more additional steps. In contrast, heterogeneous catalysis offers easier separation and reusability. However, the investigations for i-BuOH production using heterogeneous catalysts are limited.

Among those heterogeneous catalysts that have been widely utilized, hydrotalcite-derived catalysts, a class of layered double hydroxides possessing tunable properties, have emerged as promising catalysts for various chemical transformations due to their basicity, and ability to stabilize intermediate species. In the correlation with the Guerbet reaction, hydrotalcite-derived catalysts offer the potential for improved activity, selectivity, and stability [12–16]. Larina et al. [16] studied the condensation of ethanol and 1-butanol in flow reactor using Mg-Al with high productivity of 1-butanol (25 $g/(L_{cat}.h)$), and 2-ethyl-1-hexanol (19 $g/(L_{cat}.h)$, respectively. Fulong et al. [17] investigated the role of copper in $CuMgAlO_x$ for coupling of methanol/ethanol into higher alcohols products. Ni, Cu active sites are considered as effective roles for Guerbet reaction. Ni is known as an active component in methanation catalysts, as well as leading to alkylation of feedstock and/or intermediates [18, 19]. As Ni exhibits high dehydrogenation activity, increasing Ni loading would translate to the production of more aldehydes, which can then act as reactants for subsequent aldol condensation [14]. In addition, Cu species provide the basicity for the aldol condensation reaction and reduce undesirable side reaction [12,20].

This research aims to enhance knowledge and improve this sustainable method of producing i-BuOH, as well as discover the reaction route from methanol/ethanol mixture to higher alcohols by exploring the Guerbet reaction pathways using Ni/Cu-Al hydrotalcite-derived catalysts which have not been reported elsewhere. In addition, this study also helps clarify the function of Ni/Cu-Al catalysts, and the role of operating conditions. The development of higher alcohols synthesis holds promises for a more sustainable future through collaborative efforts in chemical engineering, catalysis, and the use of renewable feed stocks.

2. Experimental

2.1. Catalyst synthesis

The chemical precursors used for catalyst synthesis were Al $(NO_3)_3{\cdot}9H_2O$ (Thermo Scientific), $Cu(NO_3)_2.2{\cdot}5H_2O$ (Alfa Aesar), and $Ni(NO_3)_2{\cdot}6H_2O$ (Across Organic). First, the Cu-Al hydrotalcite support was produced with Cu:Al ratios of 3:1 and 2:1. A suitable amount of Al, and Cu was diluted in 50 mL of DI (Deionized water), then mixed in a 500 mL beaker using a magnetic stirrer (750 rpm) with total volume 200 mL. A solution of 1 M $NaOH/Na_2CO_3$ (1/1) (Thermo Scientific) continuously dropped into the mixture to get precipitated mixture and till the pH of the mixture reached around 9.3–9.5. The mixture was stirring continuously for 24 h to get completely matured. After that, the precipitated mixture was filtered using filter paper and washed to get pH around 7. The precipitated mixture was dried at 105 °C for 12 h before doping Ni catalyst on it. The hydrotalcite support with Cu-Al ratios of 2:1 and 3:1 was denoted as 2Cu-Al and 3Cu-Al, respectively.

Next, 5, 10, and 15 wt% of Ni was impregnated onto Cu-Al hydrotalcite-derived support for both ratios 2:1 and 3:1 via incipient wetness impregnation method. After that, the catalyst was dried at 105 °C for 12 h and calcined in air at 500 °C for 5 h with a ramping of 10 °C/min. The various loading of Ni on Cu-Al support was named as Ni_x/Cu-Al ($X = 5$, 10, 15). Before each experiment, the catalyst was reduced at 500 °C under H_2/Ar (4% H_2) atmosphere for 5 h with a heating rate of 3 °C/min in a tubular reactor.

2.2. Catalyst characterization

The specific surface area profiles of fresh and spent catalysts were measured using the Brunauer–Emmett–Teller (BET) and Barrett-Joyner-Halenda (BJH) methods (Gemini model, Micromeritics). The catalysts

Table 1
Experimental design for i-BuOH production using Ni/Cu-Al catalysts.

Exp	Catalyst	Cat. Loading (wt %)	Temperature (°C)	Reaction time (h)
E1	3Cu-Al	3.5	165	4
E2	2Cu-Al	3.5	165	4
E3	Ni_5O/3CuO-Al_2O_3	3.5	165	4
E4	Ni_5O/2CuO-Al_2O_3	3.5	165	4
E5	Ni_5/3Cu-Al	3.5	165	4
E6	Ni_{10}/3Cu-Al	3.5	165	4
E7	Ni_{15}/3Cu-Al	3.5	165	4
E8	Ni_5/2Cu-Al	3.5	165	4
E9	Ni_{10}/2Cu-Al	3.5	165	4
E10	Ni_{15}/2Cu-Al	3.5	165	4
E11	Ni_{10}/2Cu-Al	5.0	165	4
E12	Ni_{10}/2Cu-Al	10.0	165	4
E13	Ni_{10}/2Cu-Al	5.0	175	4
E14	Ni_{10}/2Cu-Al	5.0	185	4
E15	Ni_{10}/2Cu-Al	5.0	195	4
E16	Ni_{10}/2Cu-Al	5.0	185	10

were degassed at 90 °C for 12 h under a 1 Pa vacuum prior to measurements. Inductively Coupled Plasma combined with Optical Emission Spectroscopy (ICP-OES, Julich Research Center) was performed to measure the metal loadings (Ni, Cu, and Al). Temperature programmed-desorption (TPD) of CO_2 and NH_3 as well as temperature programed-reduction (TPR) using an AutoChem III (Micromeritics) were performed to measure the acidities, basicities, and reduction temperatures of the catalysts. Approximately 0.1 g catalyst samples were packed in a U-shaped quartz reactor, pretreated under an Ar flow (50 mL.min^{-1}) at 350 °C for 2 h, and then cooled down to room temperature. After that, the samples were purged in Ar for 1 h and then heated to 750 °C at 10 °C. min^{-1}, with an online thermal conductivity detector (TCD) recording H_2 consumption. In addition, the dispersion of different Ni catalysts also was examined via pulse CO-chemisorption method using Autochem III. About 0.1 g catalyst samples were first reduced in situ at 400 °C under 2% H_2/Ar atmosphere at a ramp rate of 10 °C min^{-1} for 1 h, then purged in Ar flow for 30 mins at 400 °C and cooled to 35 °C for 30 mins. A 2% CO/Ar mixture was used to saturate the catalyst over the course of 10 pulses, with a 5 min waiting time between consecutive pulses. The Ni dispersion was determined as $D_{Ni} = \frac{n_{CO}}{3 \times \left(\frac{x_{Ni}}{M_{WNi}}\right)} \times 100\%$ using a stoichiometry factor of Ni:CO=1 : 3 [21,22]. Here, n_{CO} represents the moles of CO uptake per mass of catalyst, x_{Ni} is the Ni loading (wt%) and M_{wNi} is the molecular weight of Ni. X-ray diffraction (XRD) diffractograms were obtained via a Bruker D8 Advance diffractometer from Bruker (Kα1(Cu), λ = 1.5406 Å), and Ni as the *Kβ*((Cu) filter) in Bragg–Brentano geometry, operating with a step size of 0.03° per second. The morphology of catalysts also examined the high-angle annular dark field (HAADF) and energy-dispersive X-ray analysis (EDX) images, an aberration-corrected FEI Titan G2 80 to 200 S/TEM field emission electron microscope was used in conjunction with a Super-X EDX system at 200 eV. Notably, the ICP-OES analysis was done using the reduced catalysts, meanwhile, all of the other measurements were conducted using calcined catalysts.

2.3. Experimental procedure

250 mg catalysts were placed in a 100 mL autoclave to evaluate the catalytic activity. The autoclave which was employed was a batch reactor including a reactor pot composed of an Inconell 600 alloy developed by Parr Instruments. Apart from the catalyst, the reactor vessel was filled with 70 mL of a mixture containing 0.45 mol.L^{-1} of NaOH, 1.6 mol.L^{-1} of EtOH, and 0.015 mol.L^{-1} of n-decane as an internal standard, and about 16 mol.L^{-1} of MeOH. After that, the autoclave was sealed and purged in a N_2 environment. The reaction temperature

Table 2
Texture profile and ICP analysis of various Ni/Cu-Al catalysts.

No	Catalyst	Ni (wt %)	Cu (wt%)	Al (wt %)	Surface Area (m^2/g)	Pore Volume (cm^3/g)	Pore Size (nm)
1	3Cu-Al	-	46.5 ± 0.8	18.0 ± 0.1	80.7	0.179	44.3
2	2Cu-Al	-	38.2 ± 0.2	14.5 ± 0.4	94.8	0.249	52.5
3	Ni_5/3Cu-Al	4.4 ± 0.1	51.6 ± 0.9	16.3 ± 0.3	45.2	0.194	50.7
4	Ni_{10}/3Cu-Al	9.5 ± 0.1	47.9 ± 0.9	15.5 ± 0.3	38.1	0.164	48.3
5	Ni_{15}/3Cu-Al	15.1 ± 1.5	43.7 ± 1.4	14.0 ± 0.5	34.8	0.160	40.2
6	Ni_5/2Cu-Al	4.9 ± 0.1	39.4 ± 0.4	18.7 ± 0.2	79.4	0.167	74.0
7	Ni_{10}/2Cu-Al	9.8 ± 0.7	37.2 ± 0.9	17.4 ± 0.2	74.0	0.111	62.4
8	Ni_{15}/2Cu-Al	15.5 ± 0.1	33.7 ± 0.5	16.0 ± 0.1	68.5	0.109	59.0
9	Spent-Ni_{10}/2Cu-Al	11.5 ± 0.6	44.0 ± 0.9	13.6 ± 0.2	5.3	0.010	37.5

was carried out at 165, 175, 185, and 195 °C. After reaching the desired temperature, 4 h of reaction time was counted. Autogenous N_2 pressure was utilized in this reaction system after purging 6 bar of N_2. The pressure varied from 18.6 to 40.5 bar, depending on the reaction temperature and reaction time. 1 mL sample was taken out every 30 mins for the gas-chromatographic analysis. The details of experimental work are shown in Table 1.

Next, the samples were collected (3 μL) using a 10 μL Eppendorf pipette (Eppendorf SE, Hamburg, Germany) and put into headspace vials (Thermo Scientific, Waltham, MA, USA). The contents of the vials were separated and examined using a gas chromatograph (Agilent 8890 GC System, Santa Clara, CA, USA) and a mass spectrometer (GC–MS, Agilent 5977B GC7MSD). The complete evaporation method was used for analysis to prevent catalyst particles from adhering to the chromatography column. A 30 m long DB-Wax column with an inner diameter of 0.25 mm and a film thickness of 0.25 μm was used for chromatographic measurement. The He flow rate of 1.2 mL.min^{-1} was used as the carrier gas. The temperature at which the GC program began, 35 °C, remained constant for 4 mins. Next, the mixture was heated to 200 °C at a rate of 20 °C per minute. Again, this temperature was maintained for 4 mins. The reaction products were quantified using calibration solutions that were prepared from the pure ingredients. The internal standard was N-decane. The concentration of products was measured through GCMS and calibration steps. After reaction, the reactor was cooling down to room temperature, and the reaction mixture was separated using a filter paper (pore diameter =0.8 μm) to collect the spent catalyst. The spent catalyst was washed with ethanol and dried at 105 °C before further characterizations.

Ethanol conversion (X_E) was determined using Eq. (1). In this equation, c_K reflects the concentrations of the different products of the Guerbet reaction, while Z stands for their stoichiometric coefficients. Specifically, the stoichiometric coefficient for the formation of i-BuOH was one, whereas those for the generation of 1-butanol and 1-hexanol were two and three, respectively. Notable, there are small gas products after reaction which are neglectable (including CO, CO_2, H_2, CH_4, and C_2H_4). Therefore, the conversion was calculated only based on the liquid products.

$$X_E = \frac{\sum_{k=i}^{n} c_k \times Z}{c_{E,\ t=0}} \times\ 100\ (\%) \quad (1)$$

For selectivity S_i of a specific component "i" as well as the space–time yield of i-BuOH (STY), the following equations were formulated:

Table 3
Pulse CO—Chemisorption analysis of various Ni/2Cu-Al catalysts.

Characteristic	Catalyst		
	Ni_5/2Cu-Al	Ni_{10}/2Cu-Al	Ni_{15}/2Cu-Al
Ni Metal dispersion (%)	4.3	11.3	7.4
Metallic surface area (m^2/g metal)	28.8	60.8	49.1
Crystallite size (hemisphere) (nm)	23.4	9.0	13.7
Crystallite size (cube) (nm)	19.5	7.5	11.4

$$S_i = \frac{c_i \times Z}{\sum_{k=i}^{n} c_k \times Z} \ (\%) \tag{2}$$

$$STY = \frac{n_{(iso-ButOH)}}{m_{cat} \times t_R} \left(\frac{mmol}{h \times g}\right) \tag{3}$$

3. Results and discussion

3.1. Characterization of catalysts

Table 2 and Fig. S1 show the BET profile as well as ICP analysis of various Ni/Cu-Al catalysts. The surface area, pore volume, and pore size of Cu-Al support with ratio 3:1 were 80.7 m^2/g, 0.179 cm^3/g, and 44.3 nm, respectively. Meanwhile, the surface area, pore volume, and pore size of Cu-Al support with ratio 2:1 were 94.8 m^2/g, 0.249 cm^3/g, and 52.5 nm. Increasing Ni loading from 5 to 15 wt%, the surface area of Ni/Cu-Al catalysts decreased from 45.2 to 34.8 m^2/g (ratio 3:1) and from 79.4 to 68.5 m^2/g (ratio 2:1), respectively. The Ni catalyst with 3Cu-Al showed a much higher pore volume compared to the catalyst with 2Cu-Al. Increasing Ni also led to decrease of the pore volume of catalyst. The pore volume decreased from 0.194 to 0.160 cm^3/g (3Cu-Al) and from 0.167 to 0.109 cm^3/g, respectively. After the reaction the surface area and pore volume of spent catalyst Ni_{10}/2Cu-Al significantly decreased from 74.0 to 5.3 m^2/g, and from 0.111 to 0.010 cm^3/g, whereas, the pore size decreased from 62.4 to 37.5 nm, respectively.

The series of Ni loading was validated by ICP analysis (Table 2), which showed that measured values closely matched nominal compositions. Despite having a high metal loading, the Ni_{15}/3Cu-Al catalyst showed successful impregnation with a Ni content of 15.1 ± 1.5 wt%. In both catalyst groups, nickel deposition followed nearly linear relationships: 2Cu-Al catalysts reached 4.9 → 9.8 → 15.5 wt% Ni, while the 3Cu-Al series demonstrated 4.4 → 9.5 → 15.1 wt% Ni advancement, respectively. In the spent-catalyst, the Ni content slightly increased from 9.8% to 11.5%, and the Cu content increased from 37.2% to 44.0%, respectively. Whereas the Al content decreased to 13.6%, most likely because the deviation during measurement. The was a concern about Al_2O_3 might react with NaOH via alkaline leaching under pressure condition during reaction operating conditions and formed $NaAlO_2$ following equation $NaOH + Al_2O_3 \rightarrow NaAlO_2 + H_2O$ [23]. However, the amount of Al_2O_3 decreased relatively low (3.8 wt%) it indicated that the catalyst structure was stable under the elevated pressure at 185 °C.

Table 3 presents metal dispersion of Ni/2Cu-Al catalysts via CO-chemisorption. Compared to its Ni_5 (4.3%) and Ni_{15} (7.4%) equivalents, the Ni_{10}/2Cu-Al catalyst shows greater metal dispersion at 11.3%, respectively. The maximum metallic surface area of 60.8 m^2/g metal for the Ni_{10} formulation results from this ideal dispersion; this is significantly larger than Ni_{15}/2Cu-Al (49.1 m^2/g metal) and more than double that of Ni_5/2Cu-Al (28.8 m^2/g metal). The smallest crystallite sizes, calculated at 9.0 nm for hemispherical and 7.5 nm for cubic morphologies, are correlated with the improved dispersion and surface area of Ni_{10}/2Cu-Al. It's interesting to note that the Ni_{15}/2Cu-Al catalyst exhibits intermediate values for every parameter, indicating that particle agglomeration and decreased active surface area occur when the nickel content is increased over 10 wt% loading. These findings imply that 10 wt% Ni is the ideal composition for optimizing the amount of metallic surface available in this catalyst series.

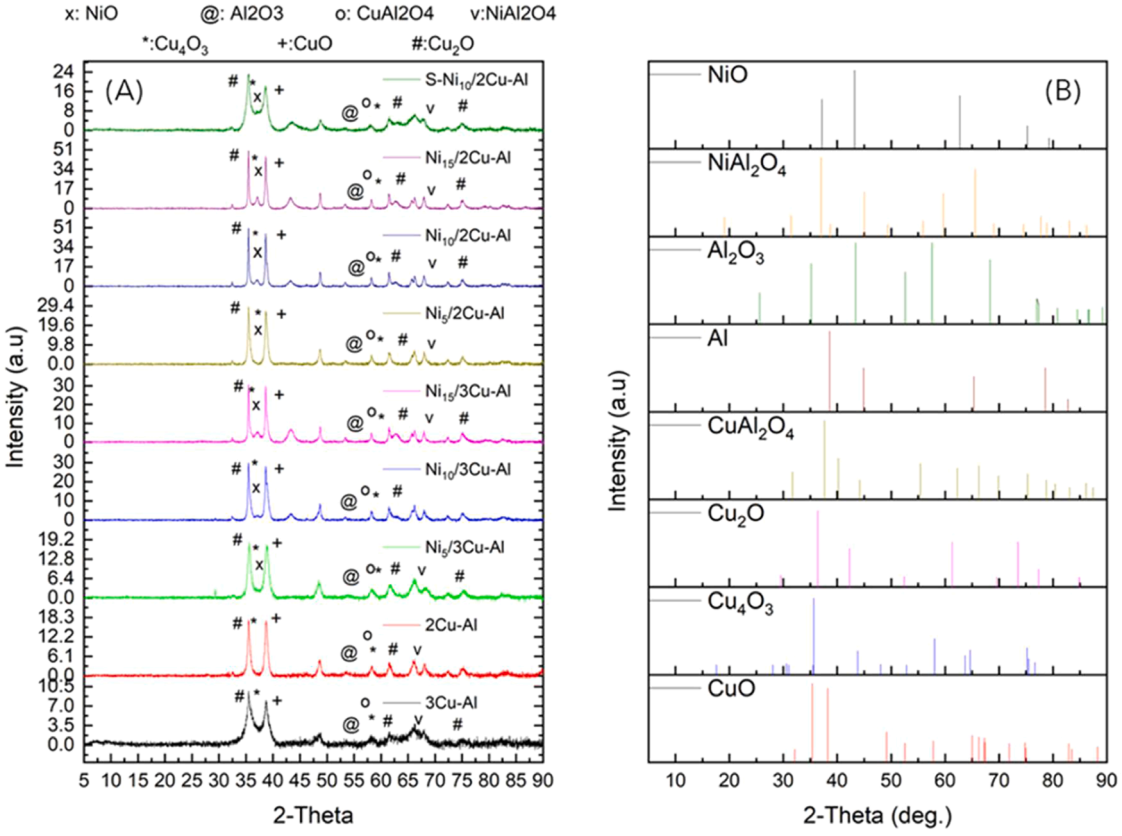

Fig. 1. (A) XRD patterns, and (B) relevant phase structures of hydrotalcite-derived Ni/Cu-Al catalysts.

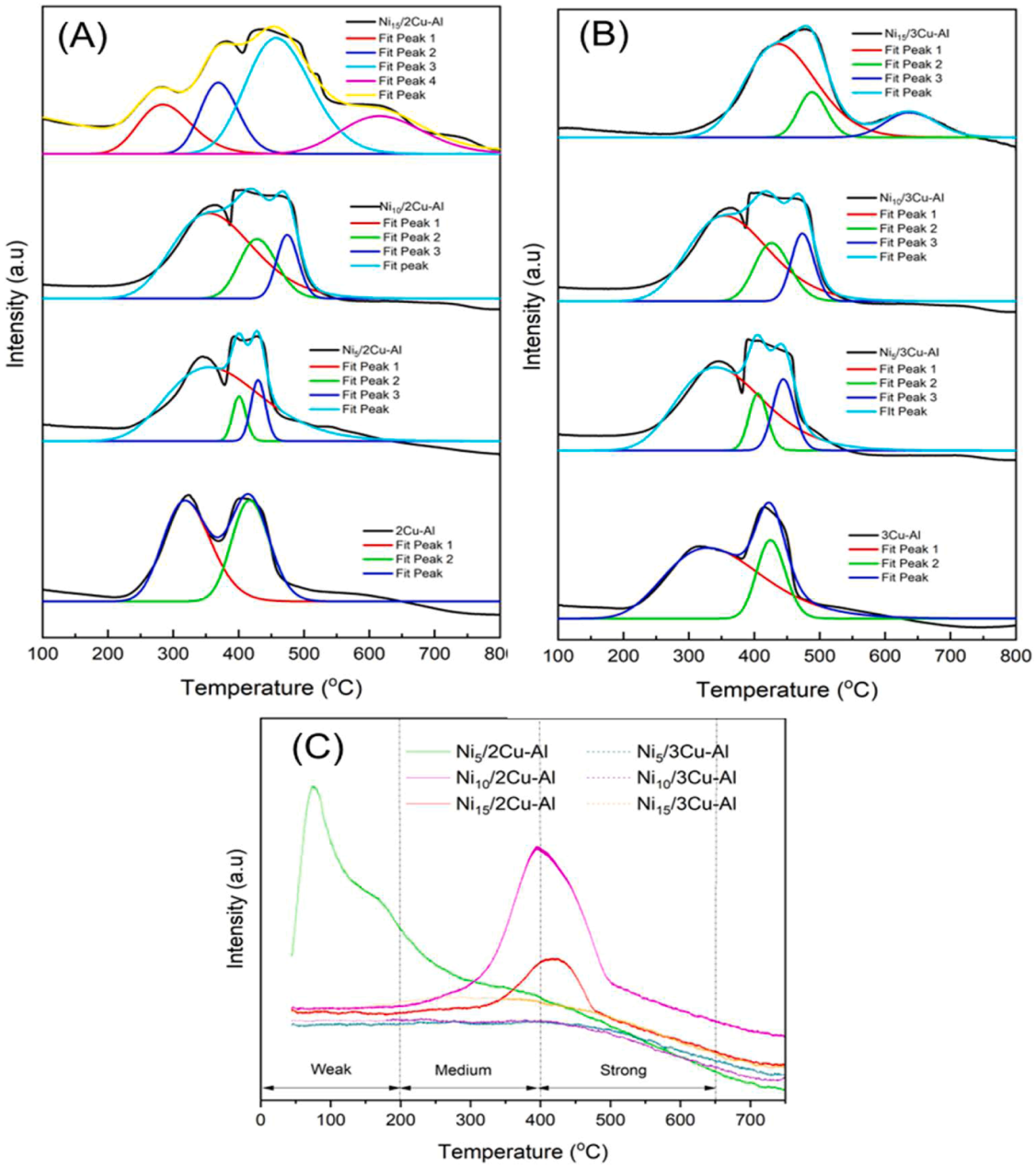

Fig. 2. Temperature programmed: (A, B) NH_3-TPD, (C) CO_2-TPD of various Ni/Cu-Al hydrotalcite-based catalysts.

The temperature programmed reduction profiles (TPR) are presented in Fig. S2. The large peak at about 390 °C corresponds to Cu. The lower reduction temperature of Cu^{2+} to Cu^0 was found by Sonobe et al. [24] (at 350 °C) with the H_2 reduction of Copper oxide subnanoparticles. Whereas, the higher reduction temperature of Cu^{2+} to Cu^0 was found by Yuan et al. [7] (at about 410 °C) with the H_2 reduction of Nitrogen-doped Carbon decorated Cu catalyst. Meanwhile, the small flat peak at about 550 °C corresponds to Ni. Pasel et al. [25] reported the lower temperature reduction of Ni at around 470 °C with NiPt/C. The shifting of temperature reduction depends on the structure and materials of catalyst. The peak of Ni reduction was clearer on HTC 2Cu/Al than 3Cu/Al due to the ratio of Ni/Cu in the catalysts. Increasing of Ni loading from 5 to 15 wt%, the reduction temperature slightly shifted to higher temperature from 550 to 570 °C.

The XRD pattern of Ni/Cu-Al are shown in Fig. 1A-B. The peaks at 37.0 and 42.3° correlate to γ-Al_2O_3 which is commonly found in Al-hydrotalcite derived catalyst. The peak at 37.1° and 65.3 ° represente Al_2NiO_4. The detection of Al_2O_3 and Al_2NiO_4 phases indicate the successful incorporation of aluminum in the catalyst structure, which can enhance thermal stability and dispersion of active metal particles. The Al_2NiO_4 spinel formation suggests strong interaction between nickel and the alumina support. Meanwhile, the presence of multiple copper oxide phases such as CuO (35.5, 38.7, 48.9, 66.4, and 75.1°), Cu_4O_3 (36.0, 44.8, and 58.0°), and Cu_2O (36.2, 42.1, and 61.1°) suggest incomplete or non-uniform oxidation of copper during the catalyst preparation or treatment process. The presence of NiO peaks at 37.1, 43.2, 63.0, 76.0, and 79.5° confirms the successful incorporation of nickel in the catalyst. The crystalline nature of NiO particles may affect the catalyst's activity and selectivity in Guerbet reactions. Compared to fresh 10Ni/2Cu-Al, the Cu and Ni in spent catalyst S-10Ni/2Cu-Al transform into oxidic forms such as Cu_2O, CuO, Cu_4O_3, and NiO. Through the X-ray diffraction of spent catalyst which collected after the reaction, there was no existence of Na in Ni/Cu-Al phase structure. This result supported the hypothesis of stable structure of Ni/Cu-Al under reaction conditions in this

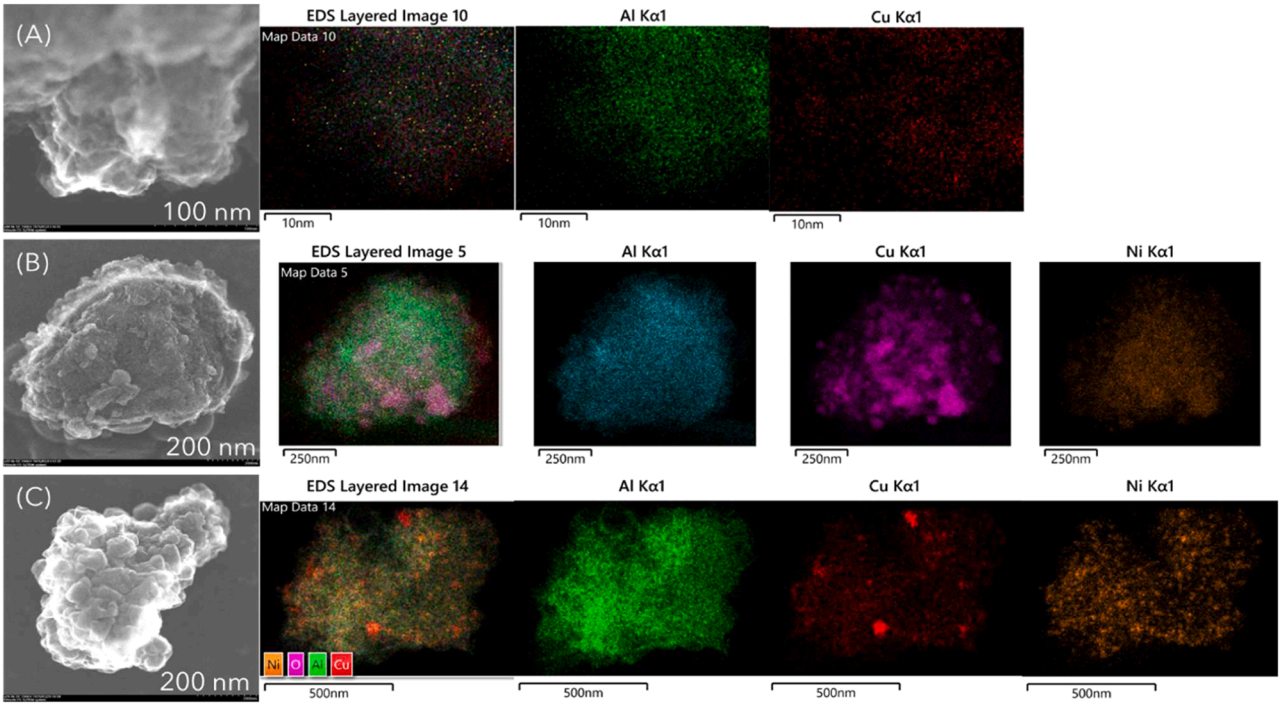

Fig. 3. S/TEM-EDX dot mapping of (A) 2Cu-Al support, (B) Ni_{10}/2Cu-Al, and (C) Spent catalyst S-Ni_{10}/2Cu-Al.

study. Via XRD pattern of reduced Ni10/2Cu-Al (Fig. S3), there was high intensity of Cu species at 43.3, 50.5, 74.2°, respectively. Meanwhile, there was no clear evidence of Ni and spinel Al_2NiO_4 on the diffraction of the catalyst. However, there were phase structures of Ni at 44.4, 51.7, 76.2° and spinel Al_2NiO_4 at 31.8, 34.7, 36.9, 38.7, 42.5, 43.8, 48.5, 56.0, 63.9, 64.8, 67.0, 69.9°, respectively. It indicates that both Ni and Al_2NiO_4 were well-contributed on the surface of the catalyst. Via XRD pattern of reduced Ni_{10}/2Cu-Al, there was high intensity of Cu species at 43.3, 50.5, 74.2°, respectively. Meanwhile, there was no clear evidence of Ni and spinel Al_2NiO_4 on the diffraction of the catalyst. However, there were phase structures of Ni at 44.4, 51.7, 76.2° and spinel Al_2NiO_4 at 31.8, 34.7, 36.9, 38.7, 42.5, 43.8, 48.5, 56.0, 63.9, 64.8, 67.0, 69.9 °, respectively. It indicates that both Ni and Al_2NiO_4 were well-contributed on the surface of the catalyst. The spinel $NiAl_2O_4$, and $CuAl_2O_4$ have the Lewis acidity which can lead to C—C formation and thus produce higher alcohols. In more detail, the spinel $NiAl_2O_4$, and $CuAl_2O_4$ contain Al^{3+} ions occupy octahedral and/or tetrahedral sites, while Ni^{2+}/Cu^{2+}ions occupy the remaining lattice positions.

Fig. 2 indicate both (A, B) NH_3 and (C) CO_2 temperature programmed desorption (TPD) profiles. The NH_3 desorption represents the potency of catalyst's acid sites. Whereas the CO_2 desorption correlates to the basicity degree of catalysts [26]. The acid sites of catalysts affect and contribute to the isomerization/alkylation and dehydration reactions [27]. The desorption of NH_3 at a low temperature (<250 °C) represents weak acidity, while the peak at 250–400 °C indicates medium and at 400–650 °C represents strong acidity. Meanwhile, the basic sites indicate the carbon coupling (C—C), dehydration, and dehydrogenation which are suitable for longer chain alcohols synthesis [28]. Through the Cu-Al hydrotalcite support, there are 2 peaks at 320 and 410 °C which relate to medium and strong acidity. The contribution of Ni to the acidity is visible in the peak at about 440 °C which indicates strong acidity. The metal species also play a vital role in dehydrogenation and rehydrogenation reactions. These reactions are involved in the Guerbet coupling reaction (initial dehydrogenation and final rehydrogenation step) [29,30]. Herein, the combination of Ni and Cu active sites could lead to high catalytic activity and reduce undesirable products. The Ni and Cu active sites could attract the H_2 molecules and activate H2 into H* species, thus directly affecting the dehydrogenation in OH group. Meanwhile, the weak/medium acidity can stabilize $C = O$ bond and make the H* easier to attack and form OH after the condensation. Consequently, the conversion and selectivity of i-BuOH would be improved. The basic sites can be classified as: (i) weak (50–200 °C), (ii) intermediate (200–400 °C), and (iii) strong (400–650 °C) basic sites [31]. The Ni/2Cu-Al samples indicate the peak with weak basicity at 80 °C (Ni_5), medium/strong basicity at around 400 °C (Ni_{10}) and strong basicity at 420 °C (Ni_{15}). Meanwhile, Ni/3Cu-Al showed no peak according to basicity compared to Ni/2Cu-Al. The weak and medium basic sites are favored for aldol condensation, whereas the strong basic sites are favored for the formation of side reactions [12,32].

The morphology of 2Cu-Al, Ni_{10}/2Cu-Al, and S-Ni_{10}/2Cu-Al catalysts and the distribution of Ni, Cu, Al were examined via S/TEM-EDX mapping (Fig. 3 (A-C)). In addition, the uniform elemental dispersion of Ni/Cu-Al also was presented. Combined with XRD pattern and S/TEM picture, the 2Cu-Al and Ni_{10}/2Cu-Al catalysts all possessed a regular structural morphology as segregated phases. On the surface of both catalysts, large granular crystals appeared, which might occur by the precipitation of active metals during the calcination/reduction of the catalysts. The Ni particle size was 8.17 nm which was determined using TEM (Fig. S4), combined with Image J software. This value is correlated with CO chemisorption result.

3.2. Catalytic activity of various Ni/Cu-Al hydrotalcite-derived catalysts

3 experiments as control experiments were conducted to confirm the role of catalysts in this study: the blank experiment (without both Ni/Cu-Al catalyst, and NaOH) and another one experiment with NaOH, without Ni/Cu-Al catalyst, both gave no products in liquid phase. Meanwhile, the 3rd experiment with Ni/Cu-Al (without NaOH) led to formation of acetaldehyde, 1,1-dimethoxyethane, Methyl formate, and Methyl acetate as major products. By using low reaction temperature, it cannot fully activate the medium/strong basicity (upper 200 °C) as well as Lewis acidity from Ni/Cu-Al catalysts, and thus, the aldol condensation by Ni/Cu-Al is not favorable. The role of NaOH in this study is a support for aldol condensation reaction when the reaction temperature is

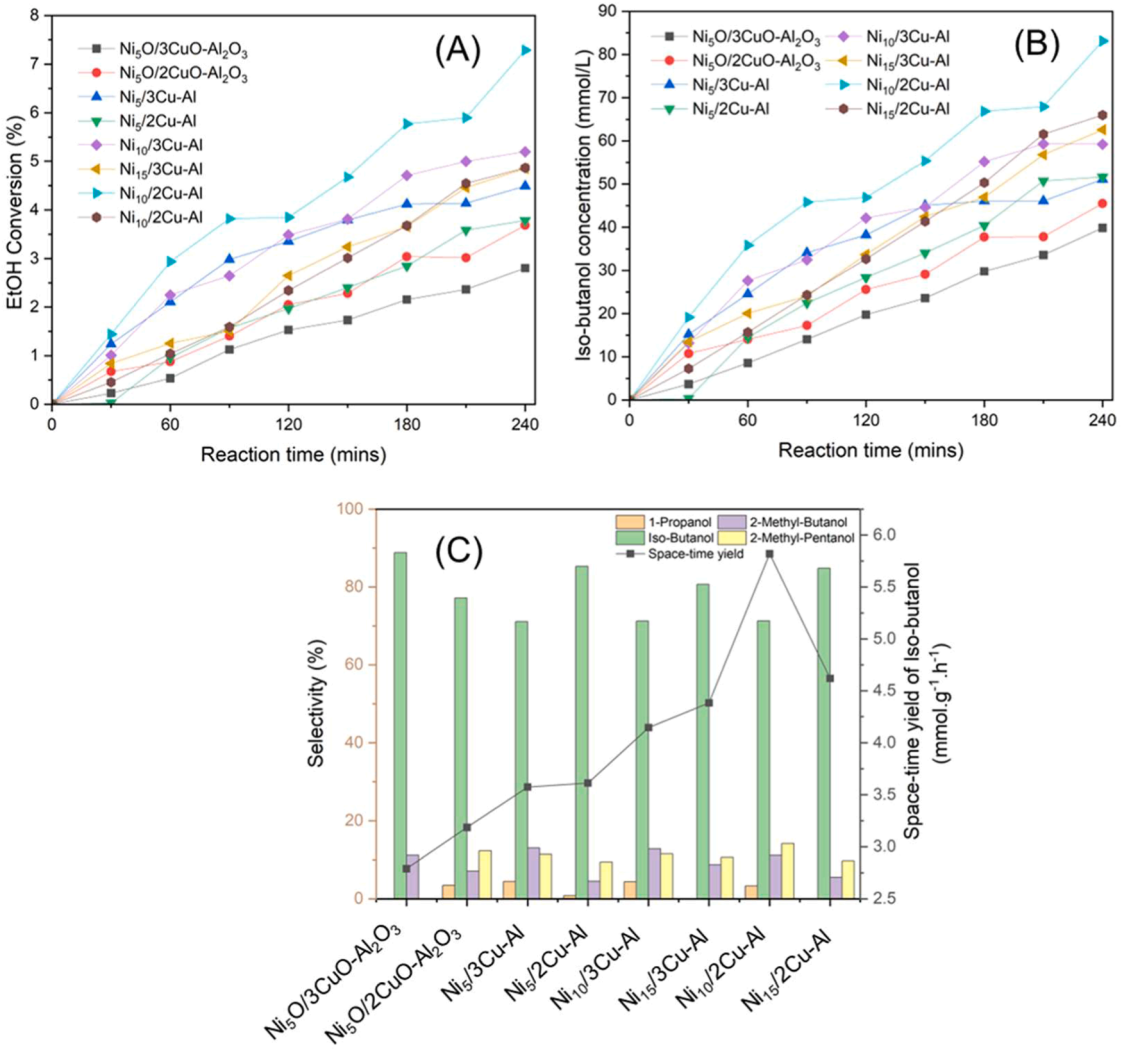

Fig. 4. Effect of various Ni/Cu-Al (3.5 wt%) hydrotalcite-based catalysts at 165 °C, 6 bar N_2 (room temperature) and 4 h reaction time: (A) EtOH Conversion, (B) i-BuOH concentration, and (C) Selectivity of higher alcohols products, and Space-time yield of i-BuOH at 4 h of reaction time.

relatively low.

The Cu-Al support with ratios 2:1 and 3:1 showed approximately no effect on the higher alcohols production at 165 °C, 6 bar of N_2 (room temperature) and 4 h reaction time. There was negligible trace Mass Spectroscopy signal of i-BuOH. Fig. 4 (A-C) shows the effect of various Ni/Cu-Al catalysts on Guerbet reaction. Using Ni/Cu-Al, the mixture of methanol/ethanol was converted into 1-propanol, i-BuOH (main product), 2-methyl-butanol, and 2-methyl-pentanol. There was no 1-butanol found in the liquid products. On experiment E3 and E4, with the use of $Ni_5O/3CuO\text{-}Al_2O_3$ and $Ni_5O/2CuO\text{-}Al_2O_3$, the conversion of EtOH was 2.8 and 3.7%, respectively. At 165 °C and 4 h reaction time, the methanol/ethanol mixture was converted into 39.8 and 45.5 mmol/L of i-BuOH with the selectivity of 88.8 and 71.2%, respectively. Except i-BuOH as the main product using Ni/Cu-Al, methanol/ethanol also was converted into 1-propanol, 2-methyl-1-butanol, and 2-methyl-pentanol. The 2Cu-Al support showed better performance compared to 3Cu-Al when Ni was impregnated onto them. On E5-E10, the various Ni loadings from 5 to 15 wt% were doped on both 2Cu-Al and 3Cu-Al to figure out the catalytic effect. The same trend was observed with the highest conversion and i-BuOH concentration using 10Ni loading on both 2Cu-Al and 3Cu-Al supports. With 5, 10, 15 wt% Ni loading on 2Cu-Al, the EtOH conversion was 3.8, 7.3, and 4.9%, respectively. Meanwhile, with 5, 10, 15 wt% Ni loading on 3Cu-Al, the EtOH conversion was 4.5, 5.2, and 4.9%, respectively. This result was in good agreement with dispersion analysis via CO—Chemisorption (Section 3.1). Among E5-E10 experiments, the highest concentration of i-BuOH was achieved at 83.1 mmol/L using 10Ni/2Cu-Al with 71.3% of selectivity and 5.8 $mmol.g^{-1}.h^{-1}$ of space-time yield. Ly et al. [33] also observed a similar trend on hydrodeoxygenation of 2-furyl methyl ketone using different Ni loadings on γ-Al_2O_3. In Ly's study, 10 wt% Ni loading facilitated the uniform dispersion of Ni on the support surface for catalytic active sites. In contrast, loading more Ni might lead to particle agglomeration of metal particles, and/or create Ni oxide clusters or bulk Ni oxides, thus, reduce the exposure of Ni active sites and lower the catalytic activity. Tran et al. [34] obtained the comparable results using 10 wt% of both Ni/γ-Al_2O_3 and Fe/AC for deoxygenation of guaiacol.

3.3. *Effect of different temperature and catalyst amount using Ni_{10}/2Cu-Al catalyst*

Ni_{10}/2Cu-Al was further chosen for investigating the effect of catalyst amount (Fig. 5 (A-C)). When the ratio catalyst/feedstocks increased from 3.5 to 5.0 and to 10.0 wt%, the EtOH conversion increased from 7.3 to 8.2 and then decreased to 5.2%, respectively. The i-BuOH concentration increased from 83.1 (3.5 wt% cat.) to 103.6 mmol/L (5.0 wt% cat.), then decreased to 60.7 mmol/L, respectively. Meanwhile, the space-time yield of i-BuOH decreased from 5.8 (3.5 wt% cat.) to 5.2 (5.0 wt% cat.), and to 1.5 $mmol.g^{-1}.h^{-1}$ (10.0 wt% cat.), respectively. The

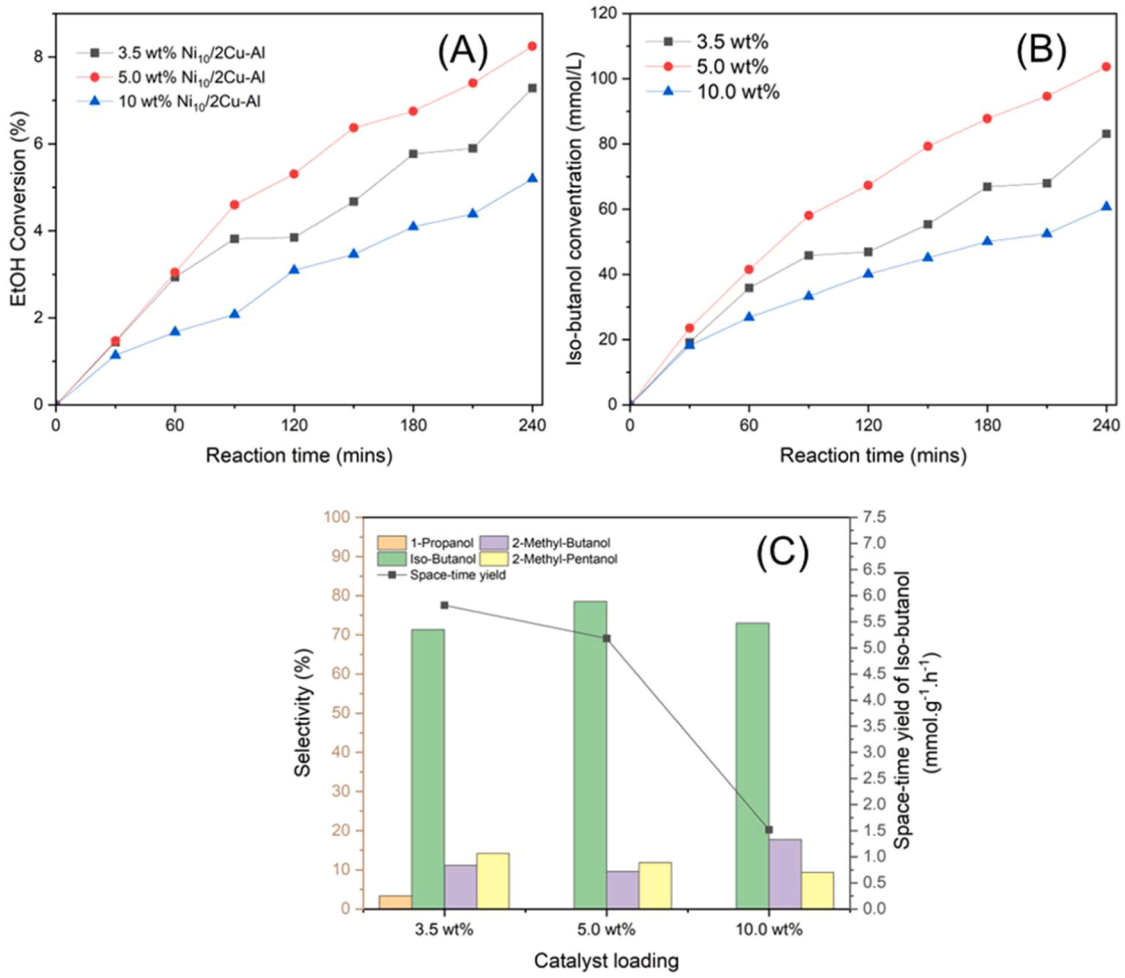

Fig. 5. Effect of catalyst loading using Ni_{10}/2Cu-Al at 165 °C, and 4 h reaction time: (A) EtOH Conversion, (B) i-BuOH concentration, and (C) Selectivity of higher alcohols products, and Space-time yield of i-BuOH at 4 h of reaction time.

selectivity of i-BuOH was 71.3 (3.5 wt% cat.), 78.6 (wt% cat.), and 73.0% (10.0 wt% cat.), respectively. Increasing the catalyst loading amount in the reaction can increase the activity by increasing the contact between the reactants and catalyst, providing more active sites for the reaction. However, when too much catalyst is added, the diffusion of reactants to the active sites can become limited. The reaction may become controlled by the rate of mass transfer rather than the intrinsic activity of the catalyst, reducing the overall reaction efficiency [35]. In addition, high catalyst amount may lead to particle aggregation or active site blocking (overcrowding), which reduces the effective surface area of the catalyst and thus lowers the number of available active sites [36].

5.0 wt% of Ni_{10}/2Cu-Al was used for further investigation of the effect of reaction temperature (Fig. 6 (A-C)). Increasing the reaction temperature from 165 to 185 °C, the EtOH conversion, and i-BuOH concentration at 4 h reaction time increased from 8.3 to 11.4%, and from 103.7 to 156.4 mmol/L, respectively. The i-BuOH selectivity varied from 78.6 to 85.8%, respectively. The reaction showed highest activity at 185 °C. Yuan et al. [37] show the same trend with the EtOH increased from 32.9 to 73.7% when the reaction temperature increased from 200 to 300 °C. Pasel et al. [38] also achieved the highest conversion of EtOH at 180 °C with a case study from 150 to 180 °C using NiPt/C. Cheng et al. [15] showed the formation of C_3+C_4 aldehydes in the research of methanol/ethanol reaction using $CuMgAlO_x$ at 260 °C and 1 bar N_2. However, the ethanol conversion was similar at 185 and 195 °C and remained at 11.4%, respectively. At 195 °C, the i-BuOH concentration, as well as the i-BuOH selectivity decreased to 112.9 mmol/L and to 60.6%, respectively. The space-time yield of i-BuOH increased from 5.0 to 7.6 $mmol.g^{-1}.h^{-1}$ (165–185 °C), then decreased to 5.5 $mmol.g^{-1}.h^{-1}$ (195 °C), respectively. At high temperatures the i-BuOH was further oxidized and converted into isobutyl aldehyde. The concentration of isobutyl aldehyde was 39.8 mmol/L, respectively. In agreement, Yuan et al. [37] confirmed the formation of acetaldehyde, 2-ethyl hexanal during ethanol upgrading to higher alcohols using NiO-modified Cu-based component (Cu–NiO) with a Mg–Al–Zr mixed metal oxide component (MgAlZrO) under reaction condition of 250 °C, and 20 bar N_2. Notable, at 185 °C and from 2 h to 4 h of reaction time, the conversion as well as the i-BuOH concentration remained similar. In addition, the use of 5.0 wt% Ni/2Cu-Al at 185 °C (E16) prolonged the reaction time to 8 h (Fig. S5) to check the reaction phenomena. From 4 to 8 h, the concentration of i-BuOH was not changed. It indicated that the reaction from methanol/ethanol into i-BuOH using 10Ni/2Cu-Al reached equilibrium after 4 h at 185 °C and 6 bar of N_2. To clarify the regeneration of the catalyst, 2 different methods were utilized and described on Supplemental Information (Fig. S6).

Compared to the net calorific value (NCV) of methanol (19.5 MJ/kg) and ethanol (26.8 MJ/kg) in the feedstocks which are presented in Fig. 6 -D, the liquid products which contains higher alcohols (C_3–C_6) has much higher NCV such as 1-propanol (30.7 MJ/kg), i-BuOH (33.1 MJ/kg), 2-methyl-butanol (34.5 MJ/kg), and 2-methyl-pentanol (35.8 MJ/kg) [5]. In this research, the methanol/ethanol mixture with input NCV was 20.2 MJ/kg while after reaction, the NCV of liquid products (excluding remaining methanol/ethanol) increased to 33.1 MJ/kg, respectively. Therefore, the liquid product can be utilized as high-quality blend fuel

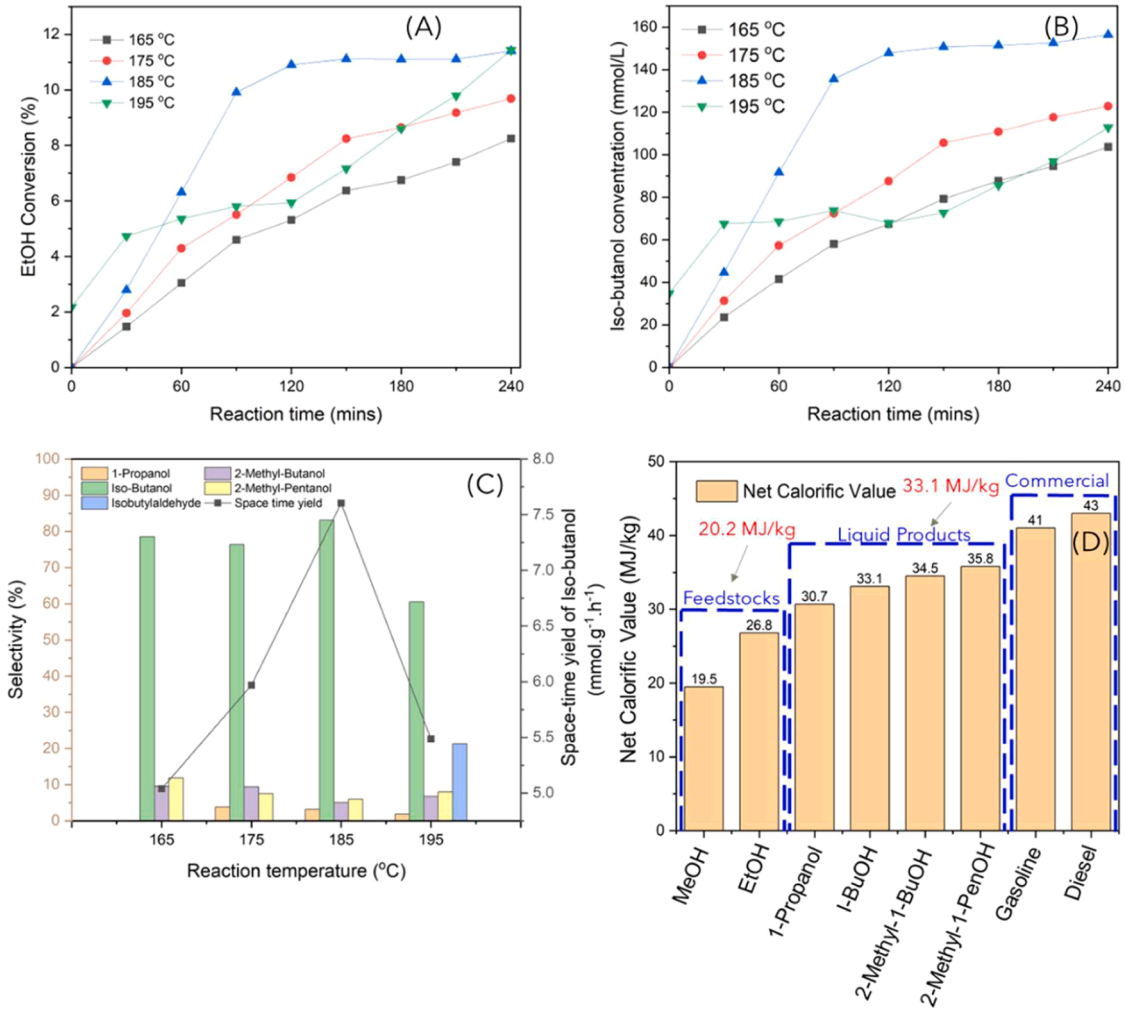

Fig. 6. Effect of reaction temperature using 5.0 wt% of Ni_{10}/2Cu-Al, 6 bar of N_2, and 4 h reaction time: (A) EtOH Conversion, (B) i-BuOH concentration, (C) Selectivity toward higher alcohols products, and Space-time yield of i-BuOH at 4 h of reaction time, (D) Net Calorific of feedstocks and products.

for gasoline compared to E10 fuel in the market.

The reaction pathways of methanol/ethanol mixture using Ni/Cu-Al hydrotalcite-based catalyst were also determined by the liquid products (Scheme 2). The first stage of this reaction pathway was dehydrogenation. Both methanol and ethanol were dehydrogenated into formaldehyde and acetaldehyde. Then those aldehydes quickly reacted with one another via aldol condensation reaction and hydrogenation to produce higher alcohol. 1 mol of acetaldehyde reacted with formaldehyde to form 1-propanal, then the 1-propanal was hydrogenated to produce 1-propanol. Instead of hydrogenation reaction, 1-propanal also can react with 1 mol formaldehyde to form 2-methyl-propenal. After that 2-methyl-propenal was hydrogenated into i-BuOH. Meanwhile, 2 mol of acetaldehyde could be coupled and hydrogenated to form 1-butanol. Like i-BuOH, other higher alcohols such as 2-methyl-butanol, and 2-methyl-1-pentanol were produced via aldol condensation of 1-butanal/2-methyl-butanal with formaldehyde and hydrogenation reaction. The i-BuOH was dehydrogenated and converted into isobutyl aldehyde (at 195 °C).

Combining Scheme 2, Table S2, and formular (S1-S5), the dehydrogenation, C—C formation, and hydrogenation rate were determined and shown on Table 4. The total dehydrogenation varied from 8.6 to 24.5 mmol.g^{-1}.h^{-1}, respectively. Meanwhile, the EtOH dehydrogenation was from 3.0 to 8.6 mmol.g^{-1}.h^{-1}, respectively. The C—C formation varied from 0.4 to 1.7 mmol.g^{-1}.h^{-1}, respectively. The hydrogenation was from 3.4 to 16.3 mmol.g^{-1}.h^{-1}, respectively. At optimized condition, the EtOH dehydrogenation, total dehydrogenation, C—C formation, and hydrogenation were 8.6, 24.5, 1.7, and 16.3 mmol.g^{-1}.h^{-1}, respectively. Through Table 4, the adjustment of MeOH/EtOH ratio and the amount NaOH can be easily determined for better achievement on EtOH conversion and selectivity of i-BuOH. In more detail, these results suggest that the ratio of MeOH/EtOH, and NaOH should be decreased.

Table 5 presents the comparison between this current work and other literature with the operation conditions and results based on space-time yield of i-BuOH and i-BuOH concentration. There are just a few studies that focus on i-BuOH production using heterogeneous catalysts. The work of Carlini et al. [39] showed the i-BuOH selectivity of 98.4% using $CuCr_2O_4$/MeONa at high H_2 pressure (81 bar) and 200 °C. Meanwhile, Li et al. [2] presented high EtOH conversion at 85% with 65% of i-BuOH selectivity under 20 N_2 and 250 °C, respectively. The results of Liu et al. [4] showed about 53.0% EtOH converted to i-BuOH with selectivity of 90% under air condition and 160 °C. Notable, the use of catalyst is important for i-BuOH production. However, the operation conditions also play a vital role. In addition, the ratio of catalyst/feedstocks and/or base/feedstocks also have a strong effect on the results which are listed in Table 4. It suggests that high temperature and/or pressure as well as ratio base/feedstock should be modified for higher EtOH conversion and i-BuOH production.

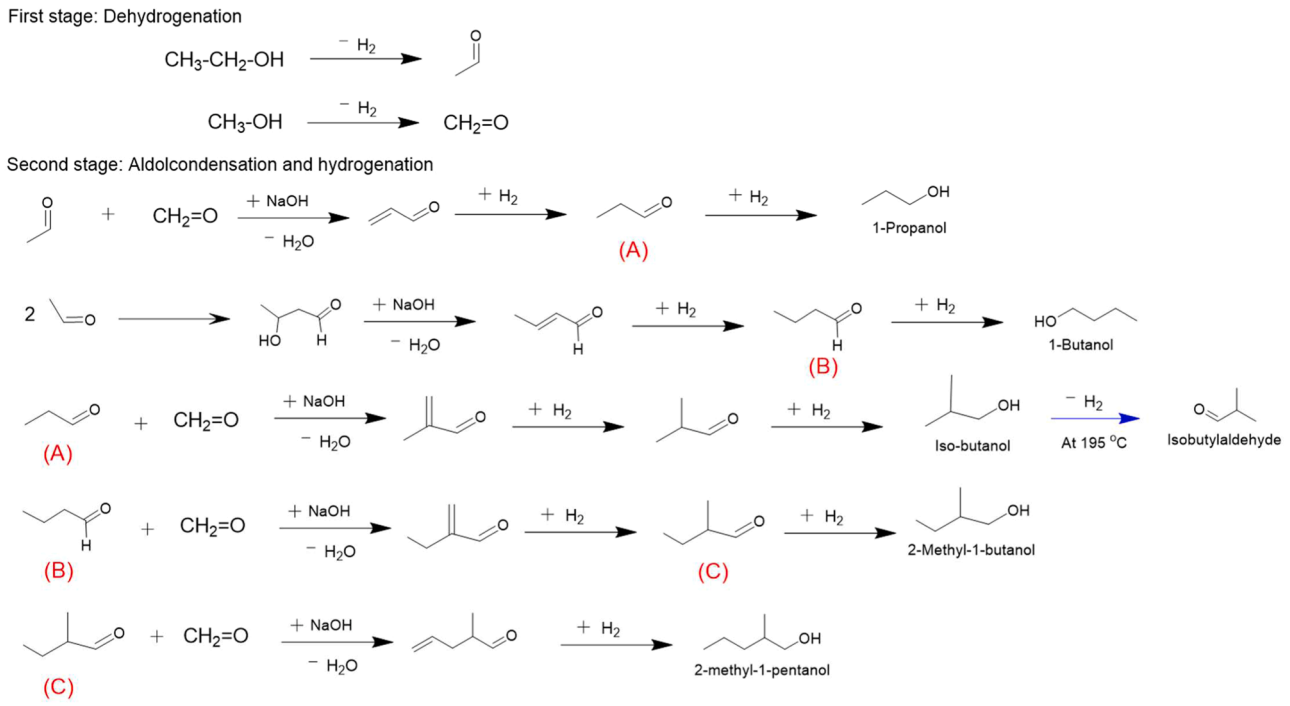

Scheme 2. Reaction pathways of methanol/ethanol upgrading using Ni/Cu-Al hydrotalcite-based catalysts.

Table 4
The measured dehydrogenation rate, hydrogenation rate and C—C formation rate over hydrotalcite-derived Cu-Al supported Ni catalysts under various experiment conditions.

Exp	Catalyst	Reaction Rate			
		EtOH Dehydrogenation ($mmol.g^{-1}.h.^{-1}$)	Total Dehydrogenation ($mmol.g^{-1}.h.^{-1}$)	C-C formation ($mmol.g^{-1}.h.^{-1}$)	Hydrogenation ($mmol.g^{-1}.h.^{-1}$)
E1	3Cu-Al	0.0	0.0	0.0	0.0
E2	2Cu-Al	0.0	0.0	0.0	0.0
E3	$Ni_5O/3CuO\text{-}Al_2O_3$	3.0	8.6	0.4	5.7
E4	$Ni_5O/2CuO\text{-}Al_2O_3$	4.0	10.9	0.5	7.2
E5	Ni_5/3Cu-Al	4.9	12.9	0.6	8.6
E6	Ni_{10}/3Cu-Al	5.6	14.9	0.7	9.9
E7	Ni_{15}/3Cu-Al	5.3	14.5	0.7	9.5
E8	Ni_5/2Cu-Al	4.1	11.6	0.5	7.6
E9	Ni_{10}/2Cu-Al	7.9	21.0	1.0	13.8
E10	Ni_{15}/2Cu-Al	5.3	14.9	0.7	9.8
E11	Ni_{10}/2Cu-Al	6.3	17.1	1.1	11.2
E12	Ni_{10}/2Cu-Al	2.0	5.2	0.7	3.4
E13	Ni_{10}/2Cu-Al	7.1	19.7	1.3	13.2
E14	Ni_{10}/2Cu-Al	8.6	24.5	1.7	16.3
E15	Ni_{10}/2Cu-Al	6.8	18.7	1.3	10.4

Table 5
STY and concentration of i-BuOH from methanol/ethanol mixture in various studies using heterogeneous catalysts.

Refernece	Catalyst	Reaction temperature (°C)	Pressure (bar) (room temp)	EtOH conversion (%)	i-BuOH concentration (mmol/L)	i-BuOH selectivity (%)
This work	Ni_{10}/2Cu-Al	185	6 (N_2)	11.4	156.4	85.8
[39]	$CuCr_2O_4$/MeONa	200	81 (H_2)	61.0	-	98.4
[2]	Cu-CeO_2/AC	250	20 (N_2)	85.0	-	65.0
[4]	Ir/N-C	160	(Air)	53.0	-	>90.0
[40]	Pt/C	150	6 (N_2)	2.24	11.9	88.9
[38]	$Ni_{99}Pt_1$/C	165	6 (N_2)	10.0	60.0	80.0
[41]	Hydroxyapatite	325	0	54.3	-	13.1

4. Conclusion

The production of i-BuOH as sustainable chemical from methanol/ethanol mixture via Guerbet reaction using Ni/Cu-Al hydrotalcite-derived catalysts was investigated in an autoclave under different conditions such as Cu-Al ratio, Ni loading, catalyst loading, temperature,

and the reaction time. The mixture of methanol/ethanol was mainly converted into i-BuOH and small amounts of 1-propanol, 2-methyl-1-butanol, and 2-methyl-pentanol. The Cu-Al hydrotalcite-derived support with Cu:Al ratio of 2:1 and 10 wt% Ni loading with higher dispersion compared to 5, and 15 wt% loading was the optimum catalyst for i-BuOH production. The experiment using Ni_{10}/2Cu-Al at 185 °C, 4 h, and 6 bar of N_2 (room temperature) showed the highest ethanol conversion at 11.4% with selectivity 100% to higher alcohols C_3—C_6, 156.4 mmol/L of i-BuOH, and 7.6 $mmol.g^{-1}.h^{-1}$ of i-BuOH space-time yield. At higher temperatures, the i-BuOH was oxidized and converted to isobutyl aldehyde. The reaction pathways of methanol/ethanol mixture into higher alcohols using Ni/Cu-Al catalysts were also proposed. Next step, the reusability/life time of catalyst will be investigated and a further scale-up process can be done to increase the higher alcohols production in continuous system at higher initial N_2 pressure to achieve better results.

Funding information

This study was funded by the Deutsche Forschungsgemeinschaft, Germany, (DFG, German Research Foundation) – 491,111,487.

CRediT authorship contribution statement

Quoc Khanh Tran: Writing – review & editing, Writing – original draft, Validation, Supervision, Methodology, Data curation, Conceptualization. **Justus Hüging:** Methodology, Investigation, Formal analysis, Data curation, Conceptualization. **Joachim Pasel:** Writing – review & editing, Supervision, Conceptualization. **Ralf Peters:** Writing – review & editing, Supervision, Funding acquisition, Conceptualization.

Declaration of competing interest

The authors declare that they have no known competing financial interests or personal relationships that could have appeared to influence the work reported in this paper.

Acknowledgements

Special thanks are due to the fuel synthesis team at Jülich Research Center and all project and cooperation partners. This work contains results obtained from the experiments performed at the Ernst Ruska-Centre (ER-C) for Microscopy and Spectroscopy with Electrons at the Forschungszentrum Jülich (FZJ) in Germany. The ER-C beam-time access was provided via the DFG Core Facility Project [FZJ_IEK-14_PJ1]. This study was funded by the Deutsche Forschungsgemeinschaft, Germany, (DFG, German Research Foundation) – 491111487.

Supplementary materials

Supplementary material associated with this article can be found, in the online version, at doi:10.1016/j.ceja.2026.101150.

Data availability

Data will be made available on request.

References

[1] R.L. Wingad, E.J.E. Bergström, M. Everett, K.J. Pellow, D.F. Wass, Catalytic conversion of methanol/ethanol to isobutanol – a highly selective route to an advanced biofuel, Chem. Commun. 52 (2016) 5202–5204, https://doi.org/10.1039/C6CC01599A.

[2] X. Li, X. Li, Continuous upgrading of methanol and ethanol to isobutanol by heterogeneous catalysis over Cu-CeO2/AC catalyst and the combination, Mol. Catal. 569 (2024) 114641, https://doi.org/10.1016/j.mcat.2024.114641.

[3] M.N.A.M. Yusoff, N.W.M. Zulkifli, H.H. Masjuki, M.H. Harith, A.Z. Syahir, L. S. Khuong, M.S.M. Zaharin, A. Alabdulkarem, Comparative assessment of ethanol and isobutanol addition in gasoline on engine performance and exhaust emissions, J. Clean. Prod. 190 (2018) 483–495, https://doi.org/10.1016/j.jclepro.2018.04.183.

[4] Q. Liu, G. Xu, X. Wang, X. Mu, Selective upgrading of ethanol with methanol in water for the production of improved biofuel—Isobutanol, Green. Chem. 18 (2016) 2811–2818, https://doi.org/10.1039/C5GC02963E.

[5] M. Peters, A. Menne, H. Gielisch, Synthesis of sustainable fuels and intermediates from ethanol and methanol, Chem. Ing. Tech. 94 (2022) 1501–1508, https://doi.org/10.1002/cite.202200020.

[6] D. Gabriëls, W.Y. Hernández, B. Sels, P. Van Der Voort, A. Verberckmoes, Review of catalytic systems and thermodynamics for the Guerbet condensation reaction and challenges for biomass valorization, Catal. Sci. Technol. 5 (2015) 3876–3902, https://doi.org/10.1039/C5CY00359H.

[7] L. Yuan, M. Zhang, G. Fan, F. Li, Remarkably boosting ethanol upgrading to higher alcohols through cooperative catalysis of surface-interface multiple-active sites on nitrogen-doped carbon decorated copper-based catalysts, Appl. Catal. B: Environ. 343 (2024) 123488, https://doi.org/10.1016/j.apcatb.2023.123488.

[8] E.S. Olson, R.K. Sharma, T.R. Aulich, Higher-alcohols biorefinery, Appl. Biochem. Biotechnol. 115 (2004) 913–932, https://doi.org/10.1385/ABAB:115:1-3:0913.

[9] F.J. Sama, R.A. Doyle, B.M. Kariuki, N.E. Pridmore, H.A. Sparkes, R.L. Wingad, D. F. Wass, Backbone-functionalised ruthenium diphosphine complexes for catalytic upgrading of ethanol and methanol to iso-butanol, Dalton. Trans. 53 (2024) 8005–8010, https://doi.org/10.1039/D4DT00561A.

[10] Y. Liu, Z. Shao, Y. Wang, L. Xu, Z. Yu, Q. Liu, Manganese-catalyzed selective upgrading of ethanol with methanol into isobutanol, ChemSusChem 12 (2019) 3069–3072, https://doi.org/10.1002/cssc.201802689.

[11] A.M. King, R.L. Wingad, N.E. Pridmore, P.G. Pringle, D.F. Wass, Rhenium complexes bearing tridentate and bidentate phosphinoamine ligands in the production of biofuel alcohols via the Guerbet reaction, Organometallics 40 (2021) 2844–2851, https://doi.org/10.1021/acs.organomet.1c00313.

[12] J. Li, L. Lin, Y. Tan, S. Wang, W. Yang, X. Chen, W. Luo, Y.-J. Ding, High performing and stable Cu/NiAlOx catalysts for the continuous catalytic conversion of ethanol into butanol, ChemCatChem 14 (2022) e202200539, https://doi.org/10.1002/cctc.202200539.

[13] J.J. Bravo-Suárez, B. Subramaniam, R.V. Chaudhari, Vapor-phase methanol and ethanol coupling reactions on CuMgAl mixed metal oxides, Appl. Catal. A: Gen. 455 (2013) 234–246, https://doi.org/10.1016/j.apcata.2013.01.025.

[14] Z. Wu, P. Wang, J. Wang, T. Tan, Guerbet reactions for biofuel production from ABE fermentation using bifunctional Ni-MgO-Al2O3 catalysts, Catalysts 11 (2021) 414.

[15] F.-l. Cheng, H.-q. Guo, J.-l. Cui, B. Hou, D.-b. Li, Guerbet reaction of methanol and ethanol catalyzed by CuMgAlOx mixed oxides: effect of M2+/Al3+ ratio, J. Fuel Chem. Technol. 46 (2018) 1472–1481, https://doi.org/10.1016/S1872-5813(18)30061-6.

[16] O.V. Larina, K.V. Valihura, P.I. Kyriienko, N.V. Vlasenko, D.Y. Balakin, I. Khalakhan, T. Čendak, S.O. Soloviev, S.M. Orlyk, Successive vapour phase Guerbet condensation of ethanol and 1-butanol over Mg-Al oxide catalysts in a flow reactor, Appl. Catal. A: Gen. 588 (2019) 117265, https://doi.org/10.1016/j.apcata.2019.117265.

[17] F. Cheng, H. Guo, J. Cui, B. Hou, H. Xi, L. Jia, D. Li, Coupling of methanol and ethanol over CuMgAlOx catalysts: the roles of copper species and alkalinity, React. Kinet. Mech. Catal. 126 (2019) 119–136, https://doi.org/10.1007/s11144-018-1476-z.

[18] X. Tang, C. Song, H. Li, W. Liu, X. Hu, Q. Chen, H. Lu, S. Yao, X.-n. Li, L. Lin, Thermally stable Ni foam-supported inverse CeAlOx/Ni ensemble as an active structured catalyst for CO2 hydrogenation to methane, Nat. Commun. 15 (2024) 3115, https://doi.org/10.1038/s41467-024-47403-4.

[19] X. Chen, Y. Zhang, C. Sun, Y. Wang, G. Song, C. Li, K. Hui Lim, R. Ye, Y. Peng, H. Arandiyan, Z.-H. Lu, G. Feng, R. Zhang, S. Kawi, Lanthanum-mediated enhancement of nickel nanoparticles for efficient CO2 methanation, Fuel 371 (2024) 131998, https://doi.org/10.1016/j.fuel.2024.131998.

[20] S. Li, X. Han, H. An, X. Zhao, Y. Wang, Improving the catalytic stability of Ni/TiO2 for ethanol guerbet condensation: influence of second metal component, Kinet. Catal. 62 (2021) 632–640, https://doi.org/10.1134/S0023158421050025.

[21] J.A. Sun, E. Selvam, A. Bregvadze, W. Zheng, D.G. Vlachos, Hydrocracking of polyolefins over ceria-promoted Ni/BEA catalysts, Green Chem. (2025), https://doi.org/10.1039/D5GC00345H.

[22] C.H. Bartholomew, R.B. Pannell, The stoichiometry of hydrogen and carbon monoxide chemisorption on alumina- and silica-supported nickel, J. Catal. 65 (1980) 390–401, https://doi.org/10.1016/0021-9517(80)90316-4.

[23] L. Grande, M.Á. Vicente, S.A. Korili, A. Gil, Synthesis strategies of alumina from aluminum saline slags, Process. Saf. Environ. Prot. 172 (2023) 1010–1028, https://doi.org/10.1016/j.psep.2023.03.006.

[24] K. Sonobe, M. Tanabe, T. Imaoka, W.-J. Chun, K. Yamamoto, Low-temperature H2 reduction of copper oxide subnanoparticles, Chem. – Eur. J. 27 (2021) 8452–8456, https://doi.org/10.1002/chem.202100508.

[25] J. Pasel, F. Woltmann, J. Häusler, R. Peters, Surface Redox Reaction For the Synthesis of NiPt Catalysts For the Upgrading of Renewable Ethanol/Methanol Mixtures, Catalysts, 2024, https://doi.org/10.3390/catal14010077.

[26] K.G. Kalogiannis, S.D. Stefanidis, S.A. Karakoulia, K.S. Triantafyllidis, H. Yiannoulakis, C. Michailof, A.A. Lappas, First pilot scale study of basic vs acidic catalysts in biomass pyrolysis: deoxygenation mechanisms and catalyst deactivation, Appl. Catal. B: Environ. 238 (2018) 346–357, https://doi.org/10.1016/j.apcatb.2018.07.016.

[27] K.N. Papageridis, N.D. Charisiou, S. Douvartzides, V. Sebastian, S.J. Hinder, M. A. Baker, A.A. AlKhoori, S.I. AlKhoori, K. Polychronopoulou, M.A. Goula,

Continuous selective deoxygenation of palm oil for renewable diesel production over Ni catalysts supported on Al2O3 and La2O3–Al2O3, RSC. Adv. 11 (2021) 8569–8584, https://doi.org/10.1039/D0RA08541C.
[28] Q.K. Tran, S. Han, H.V. Ly, S.-S. Kim, J. Kim, Hydrodeoxygenation of a bio-oil model compound derived from woody biomass using spray-pyrolysis-derived spherical γ-Al2O3-SiO2 catalysts, J. Ind. Eng. Chem. 92 (2020) 243–251, https://doi.org/10.1016/j.jiec.2020.09.012.
[29] B. Yuan, J. Zhang, Z. An, Y. Zhu, X. Shu, H. Song, X. Xiang, W. Wang, Y. Jing, L. Zheng, J. He, Atomic Ru catalysis for ethanol coupling to C4+ alcohols, Appl. Catal. B: Environ. 309 (2022) 121271, https://doi.org/10.1016/j.apcatb.2022.121271.
[30] D. Jiang, G. Fang, Y. Tong, X. Wu, Y. Wang, D. Hong, W. Leng, Z. Liang, P. Tu, L. Liu, K. Xu, J. Ni, X. Li, Multifunctional Pd@UiO-66 catalysts for continuous catalytic upgrading of ethanol to n-butanol, ACS Catal. 8 (2018) 11973–11978, https://doi.org/10.1021/acscatal.8b04014.
[31] Q.K. Tran, M.A. Salam, P.H. Ho, H.X. Le, C. Kugge, D. Creaser, L. Olsson, One-pot depolymerization of forest residues to potential aviation fuel over hybrid zeolite – N-doped activated carbon supported NiMo catalyst, Renew. Energy 246 (2025) 122835, https://doi.org/10.1016/j.renene.2025.122835.
[32] D.L. Carvalho, R.R. de Avillez, M.T. Rodrigues, L.E.P. Borges, L.G. Appel, Mg and Al mixed oxides and the synthesis of n-butanol from ethanol, Appl. Catal. A: Gen. 415-416 (2012) 96–100, https://doi.org/10.1016/j.apcata.2011.12.009.
[33] H.V. Ly, E. Galiwango, S.-S. Kim, J. Kim, J.H. Choi, H.C. Woo, M.R. Othman, Hydrodeoxygenation of 2-furyl methyl ketone as a model compound of algal Saccharina Japonica bio-oil using iron phosphide catalyst, Chem. Eng. J. 317 (2017) 302–308, https://doi.org/10.1016/j.cej.2017.02.080.
[34] Q.K. Tran, H.V. Ly, B. Kwon, S.-S. Kim, J. Kim, Catalytic hydrodeoxygenation of guaiacol as a model compound of woody bio-oil over Fe/AC and Ni/γ-Al2O3 catalysts, Renew. Energy 173 (2021) 886–895, https://doi.org/10.1016/j.renene.2021.03.138.
[35] U. Chadha, S.K. Selvaraj, H. Ashokan, S.P. Hariharan, V.Mathew Paul, V. Venkatarangan, V. Paramasivam, Complex nanomaterials in catalysis for chemically significant applications: from synthesis and hydrocarbon processing to renewable energy applications, Adv. Mater. Sci. Eng. 2022 (2022) 1552334, https://doi.org/10.1155/2022/1552334.
[36] H. Wang, W. Yu, X. Peng, Z. Chen, S. Wu, Q. Yu, W. Yang, J. Zhou, Highly efficient catalytic adsorbents designed by an “adaption” strategy for removal of elemental mercury, Chem. Eng. J. 388 (2020) 124220, https://doi.org/10.1016/j.cej.2020.124220.
[37] L. Yuan, G. Fan, L. Zheng, F. Li, Significantly boosting the production of higher alcohols from biomass-derived ethanol utilizing tandem catalysts integrating a NiO-modified Cu-based component with a Mg–Al–Zr mixed metal oxide, Green. Chem. 27 (2025) 3004–3019, https://doi.org/10.1039/D4GC05768F.
[38] J. Pasel, J. Häusler, R. Peters, D. Stolten, Catalytic activity and stability of NiPt/C catalysts for the synthesis of iso-butanol from methanol/ethanol mixtures, Catal. Sci. Technol. 14 (2024) 7048–7060, https://doi.org/10.1039/D4CY01061B.
[39] C. Carlini, M. Di Girolamo, A. Macinai, M. Marchionna, M. Noviello, A.M. Raspolli Galletti, G. Sbrana, Selective synthesis of isobutanol by means of the Guerbet reaction: part 2. Reaction of methanol/ethanol and methanol/ethanol/n-propanol mixtures over copper based/MeONa catalytic systems, J. Mol. Catal. A: Chem. 200 (2003) 137–146, https://doi.org/10.1016/S1381-1169(03)00042-6.
[40] J. Häusler, J. Pasel, F. Woltmann, A. Everwand, M. Meledina, H. Valencia, M. Lipińska-Chwałek, J. Mayer, R. Peters, Elucidating the influence of the d-Band Center on the synthesis of isobutanol, Catalysts. 11 (2021) 406.
[41] B.-C. Zhou, Q.-N. Wang, X.-F. Weng, L. He, W.-C. Li, A.-H. Lu, Regulating aromatic alcohols distributions by cofeeding methanol with ethanol over cobalt-hydroxyapatite catalyst, ChemCatChem 12 (2020) 2341–2347, https://doi.org/10.1002/cctc.202000010.